Title
CHARGED PARTICLES FROM BERYLLIUM BOMBARDED BY 31.3 -MEV PROTONS

Author
Finke, Reinald G.

Publication Date
1954-11-17

cy 2

UCRL-2789
Unclassified Physics

UNIVERSITY OF CALIFORNIA UNCLASSIFIED

Radiation Laboratory
Berkeley, California

Contract No. W-7405-eng-48

CHARGED PARTICLES FROM BERYLLIUM BOMBARDED BY 31.3-MEV PROTONS

Reinald G. Finke
(Thesis)

November 17, 1954

Printed for the U. S. Atomic Energy Commission

DISCLAIMER

CHARGED PARTICLES FROM BERYLLIUM BOMBARDED BY 31.3-MEV PROTONS

Contents

CHARGED PARTICLES FROM BERYLLIUM BOMBARDED BY 31.3-MEV PROTONS

Reinald G. Finke

Radiation Laboratory, Department of Physics
University of California, Berkeley, California

November 17, 1954

ABSTRACT

The range spectrum of charged particles resulting from the bombardment of a thin beryllium foil by 31.3-Mev protons has been measured at several angles.

In addition to previously reported energy levels in Be^9 at 2.4, 6.8, and 11.3 Mev, evidence for new levels at 5.0, 7.9, 19.9, and 21.7 Mev was obtained. The angular distribution of each of the inelastic proton groups has been analyzed on the basis of the Austern-Butler-McManus theory. In most cases this gave unambiguous answers for the angular momentum change for the reaction, assuming a reasonable nuclear radius ($a \sim 1.4\, A^{1/3} \times 10^{-13}$ cm). For the two cases in which Be^9 was left in the 19.9- and 21.7-Mev excited states, a rather large nuclear radius ($a \sim 1.7\, A^{1/3} \times 10^{-13}$ cm) was required to give a good fit. The elastic proton angular distribution is in good agreement with that given by the Born approximation.

Deuteron groups corresponding to the Be^8 ground state and first excited state were also identified. Good agreement for the angular distribution of the ground-state deuterons is found with Butler theory modified according to the proposal of Daitch and French. The group leaving Be^8 in its 3.0-Mev level is peaked forward and diminishes in cross section with increasing angle much less rapidly than any Butler prediction.

CHARGED PARTICLES FROM BERYLLIUM BOMBARDED BY 31.3-MEV PROTONS

Reinald G. Finke

Radiation Laboratory, Department of Physics
University of California, Berkeley, California

November 17, 1954

INTRODUCTION

A. Observation of Energy Levels

Excited states of a nucleus may be studied by observing scattering of charged particles by two different mechanisms. In a compound nucleus, levels above the threshold for emission of the type of particle scattered may be examined by resonance scattering, in which we may observe the variation of the cross section for elastic scattering from the target nucleus with variation in the energy of the incident particles. The binding energy of a particle to the compound nucleus determines the lowest observable amount of excitation above the ground state. Inelastic scattering gives information on all excitations above the ground state of the bombarded nucleus by indicating the amount of energy left in the target nucleus during the collision.

Inelastic scattering of protons as a means of observing excited levels of nuclei became feasible only after accelerators became capable of producing protons with energies (in the center-of-mass system) greater than the sum of the excitation energy of the level involved and the height of the Coulomb barrier of the compound nucleus. The first experiments involving this process, reported in 1940,[1,2] used protons of 6.7 and 4 Mev.

When the 32-Mev Berkeley proton linear accelerator was built, protons with several times the energies imparted by previous machines became available in sufficient quantities so that a survey could be made of the inelastic spectrum of all nuclei to well above their respective thresholds for heavy-particle emission. Inelastic scattering experiments involving carbon and aluminum,[9] beryllium and carbon,[16] helium,[19,20] and cadmium, tin, gold, and platinum,[24] have been done with this machine. As energies of accelerators have increased, so has the problem of resolving closely spaced energy levels. The levels of Al clearly

resolved by Dicke and Marshall[3] with 6.9-Mev incident protons became a hopeless blur to Levinthal, Martinelli, and Silverman,[9] even with the ultranarrow energy spread of the linear-accelerator beam. Britten[16], using a NaI(Tl) scintillation counter, obtained an energy resolution (full width at half maximum of the distribution of number vs. energy) of about 5 percent. The present detector, a differential-range proportional counter telescope, was first used in its present form by Benveniste and Cork[19, 20] and analyzed thoroughly by Ashby[21]. Energy resolution as good as 1.7 percent has been obtained for elastically scattered protons.

B. Inelastic Scattering

The mechanism of inelastic scattering is pictured in two separate ways. (1) The compound nucleus theory[10, 13] says that the incoming proton is captured by the target nucleus Z^A, forming a compound nucleus $(Z + 1)^{A+1}$ in an excited state. (See Fig. 1.) This state lasts long enough for the new proton to circulate many times (Weisskopf).[10] This or some other proton may be re-emitted with an energy equal to or lower than its initial energy. In the former case we have elastic scattering; in the latter, inelastic scattering. The difference in the center-of-mass kinetic energies of the system $(p + Z^A)$ before and after collision gives the energy left in excitation of the nucleus Z^A. The theory[13] states that protons emitted from a nucleus will have a center-of-mass angular distribution symmetrical about the angle $\pi/2$ with the incident proton velocity vector.

(2) The second picture of inelastic scattering[23] views the collision as a proton-nucleon interaction instead of a proton-nucleus interaction. In this scheme the proton does not penetrate very deeply into the nucleus nor does it stay in its vicinity longer than a time of the order of the nuclear diameter divided by the proton's velocity. Since the absorption length of a proton in nuclear matter increases with its energy, we would expect that at higher energies a proton would have more opportunity to interact with individual nucleons before becoming absorbed in compound-nucleus formation. In compound-nucleus formation at higher energies, the probability that the energy shared among all the nucleons will be reconcentrated in one nucleon becomes quite small, so that the compound-nucleus contribution to elastic scattering and inelastic scattering

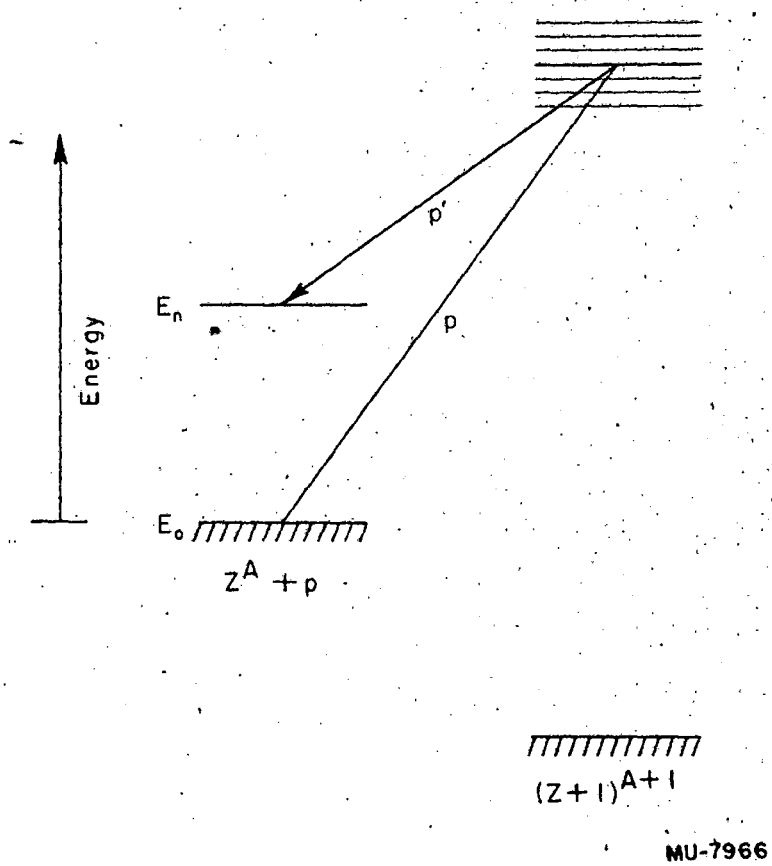

Fig. 1. Energy-level diagram of inelastic scattering of protons from target Z^A.

resulting in very low excitations goes to zero with increasing energy. Thus we would expect that the mechanism responsible for inelastic scattering would be primarily compound-nucleus formation at low energies (7.1 Mev, Davis[18]), a mixture of compound-nucleus and peripheral scattering at a higher energy (10 Mev, Fischer[25]), and predominantly peripheral scattering at a still higher energy (31 Mev, this paper). At very high excitations (low-energy outgoing particle), however, compound nucleus formation might still be expected to play an important part.

For a peripheral collision in which a nucleon, whose wave number is $\vec{k}_i$ (center of mass) before and $\vec{k}_f$ afterward, changes its angular momentum by ℓ units of $\hbar$, Austern, Butler, and McManus give for the angular distribution of the differential cross section

$$\frac{d\sigma}{d\omega} \sim \left[j_\ell \left(|\vec{k}_i - \vec{k}_f| a \right) \right]^2 ,$$

where a is the radius to the spherical shell of the nucleus in which the collision may take place, and j_ℓ is the regular spherical Bessel function of order ℓ. For backward scattering large momentum transfers are required, so the Born approximation is no longer applicable.

C. Elastic Scattering

Elastic proton angular distributions may be predicted in shape by the simple theory of Fraunhofer diffraction by an opaque disc (cf. the optical model of the nucleus[14, 7]) in cases where the effect of nuclear diffraction is many times that of Coulomb scattering. (For beryllium with 31-Mev protons the ratio to Rutherford scattering is as high as 40.) The Fraunhofer diffraction formula may be obtained by use of the Born approximation. The scattering amplitude $f(\phi)$ is given by

$$f(\phi) \sim \int \psi_f^* \; V(r) \; \psi_o \; dv,$$

where ψ_o and ψ_f are the wave functions of the incoming and the outgoing proton and have the form

$$\psi \sim e^{i\vec{k}\cdot\vec{r}} .$$

$V(r)$ is the interaction potential

$$V(r) = V_o, \quad r = a;$$

$$= 0, \quad r > a \text{ (a is the nuclear radius).}$$

dv is the volume element,

$$dv = 2\pi r^2 \sin\theta \, dr \, d\theta,$$

So,

$$f(\phi) \sim 2\pi V_o \int_o^a \int_o^\pi e^{-i\vec{k}_f \cdot \vec{r}} \, e^{i\vec{k}_o \cdot \vec{r}} \, r^2 \sin\theta \, dr \, d\theta$$

$$\sim 4\pi V_o \int_o^a \frac{\sin|\vec{k}_o - \vec{k}_f| r}{|\vec{k}_o - \vec{k}_f| r} \, r^2 \, dr$$

since

$$(\vec{k}_f - \vec{k}_o) \cdot \vec{r} = |\vec{k}_f - \vec{k}_o| r \cos\theta,$$

$$f(\phi) \sim 4\pi V_o \int_o^a j_o(gr) \, r^2 \, dr, \qquad g \equiv |\vec{k}_o - \vec{k}_f|$$

$$\sim 4\pi V_o a^3 \, \frac{j_1(ga)}{ga},$$

therefore,

$$\frac{d\sigma}{d\omega} \sim f^2(\phi) \sim \left[\frac{j_1(ga)}{ga}\right]^2 \qquad \text{(Fraunhofer diffraction)}$$

It is interesting to note that inelastic scattering is a similar diffraction phenomenon resulting from interference among the coherent waves of different angular momentum after the collision. The distribution is then characteristic of the change in angular momentum ℓ suffered by all these units of the incident-proton wave front, and is similar in form to the last integral above with the lower limit greater than zero (integration over a peripheral shell) and the order of the Bessel function equal to ℓ.

D. Deuteron Production

Deuteron production may be thought of as an inverse Butler stripping process. The Butler theory[11,22] is also concerned with a peripheral region--one of thickness less than the size of the deuteron so that one nucleon is captured and one scattered in passage by the nucleus. The angular distribution of deuteron production may be compared with that of Butler stripping by making use of the principle of detailed balance. The shape of the Butler-stripping angular distribution (see Appendix)

corresponding to the deuteron-production angular distribution gives the change in angular momentum in the reaction and a measure of the range of the nuclear forces.

E. History of Beryllium Levels

An energy level of Be^9 was first reported by Davis and Hafner in 1948[5,6] at an excitation of 2.41 Mev, observed by inelastic scattering of 7.1-Mev protons onto photographic plates at one angle (37°). This was verified by a number of other observers,[8,17] and remained the only information on the energy-level structure of Be^9 until 1952, when Davis[18] published an angular distribution for this level obtained with the above experimental means, and Britten[16] reported the results of the films of his scintillation spectrometer pulses obtained at the linear accelerator. Britten observed the inelastic spectrum of protons from beryllium at laboratory-system angles of 90°, 125°, and 160°, and reported, in addition to the first level, seeing new levels at 6.8 and 11.6 Mev. The experiment reported here was well under way at that time and had already verified the existence of these levels. An angular distribution of the differential cross section for production of deuterons from the $Be^9(p,d)Be^8$ reaction was reported by Harvey[12] in 1951.

EXPERIMENTAL APPARATUS

A. Beam Defining for Scattering

The linear accelerator beam, after leaving the last accelerating gap, has a diameter of approximately 1/4 in., an energy spread of less than 1 percent full width at half maximum, and an angular divergence of about 10^{-3} radian. The collimating system (see Fig. 2) to shape and locate the beam for scattering experiments consists (in the order that the beam traverses them) of a remotely adjustable four-jaw collimator C_1 (premagnet collimator), an analyzing magnet which bends the beam through 20°, a second manually adjustable four-jaw collimator C_2 (postmagnet collimator), and a beam-shaping collimator C_3 consisting of a 1/8-in. circular hole in a carbon disc followed 1 ft and 2 ft later by 5/32-in. and 3/16-in. holes to limit slit scattering. The size of the beam at the target is between 1/8 in. and 3/16 in., with a maximum time-average magnitude of 10^{-8} amperes. The beam-shaping collimator may be retracted, for alignment purposes, without breaking the vacuum. The beam line is initially determined by the postmagnet collimator and a picture of the beam burned into a glass plate at the exit port of the scattering chamber. The beam-shaping collimator and the scattering chamber center line are then accurately located along this line by use of a transit instrument.

B. Scattering Chamber and Equipment

The scattering chamber is the accelerator's 24-in. remotely controlled scattering chamber.[24] The 0° and 180° positions of the table as determined by the solid-angle-defining collimator mounted on the table at a radius of 6.56 in. in front of the counter telescope are accurately aligned on the beam line (see above) and are easily reproducible to 0.1°. The target-holder centering and angular calibration are also checked at each realignment of the collimating system. The remotely controlled absorber inserter between the solid-angle-defining collimator and the counter has ten solenoid-operated sliding frames with 3/4-in.-square openings Ten aluminum foil absorbers varying (in powers of 2 times 1.5 mg/cm^2) from 1.5 mg/cm^2 to 768 mg/cm^2 are mounted on these frames, permitting choice of absorber in steps of 1.5 mg/cm^2 from

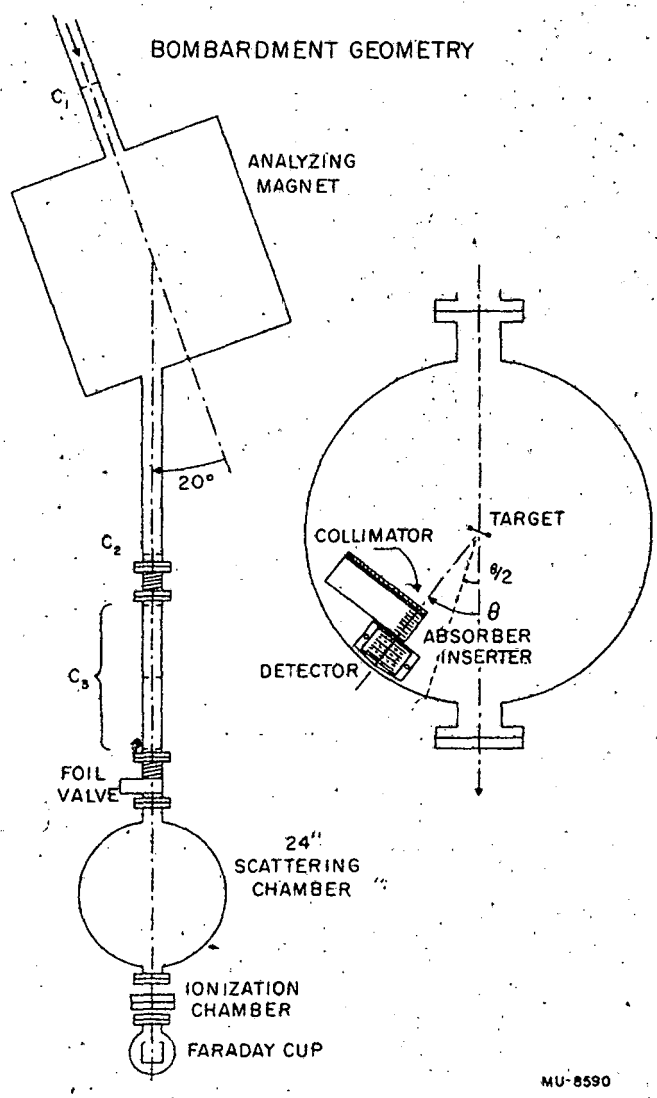

Fig. 2. Bombardment geometry

0 to 1534.5 mg/cm^2. The target is a 0.002-in. beryllium foil of thickness 11.18 mg/cm^2 with area 3/4 in. by 1 in. The vacuum in the chamber in which all the components of the range telescope are immersed is maintained by a small vacuum package (diffusion pump plus mechanical pump) at a pressure of about 10^{-5} mm Hg. Some earlier data were taken with a smaller 1-foot-diameter scattering chamber with fixed ports every 7.5° on alternate sides up to 90°. The counter and absorber inserter were mounted outside (see Benveniste[19] and Ashby[21]).

C. Counter

The counter[19,20] consists of three multiple-wire parallel-plate proportional counters, each 3/8 in. thick, separated by 1.5 and 6 mg/cm^2 Al foils and operating from a common hv supply in a common gas volume (1/2 atmosphere of 96% argon and 4% CO_2). The front window is a 1-in. circular aperture covered by a 0.001-in. dural foil. Each counter has a sensitive area greater than 1-1/2 in. square. These dimensions are sufficiently large so that protons scattered by the absorbers located between the 3/16-in.-diameter solid-angle-defining collimator and the counter do not miss the sensitive area of the last counter in any significant percentage (< 1 percent).[19] The absorbers are positioned so that the thickest is nearest the counter.

All signal and hv leads are brought into the chamber and connected with the counter in normal atmosphere inside a pressuretight channel so that the hv may be operated independently of the degree of vacuum or kind of gas (in gas-target experiments) in the chamber. Earlier experimenters experienced difficulty in preventing breakdown of voltages near 1000 v across standard hv connectors at pressures around 100 μ or in helium gas at STP.

Charged particles scattered into the solid-angle-defining collimator by the target are slowed down by the "range foil" R (absorber plus windows plus gas) and counted by each of the counters that they traverse. If we combine these pulses so that the first two are in coincidence and the last (beyond the 6 mg/cm^2 ΔR foil) in anticoincidence, we count only those particles traversing the first two counters and some part of the ΔR foil but not the last counter. In this way we can count all those particles with a range between R and R+ΔR. Particles stopping in the ΔR

foil have a dE/dx and output pulse height from the first two counters many times as large as those particles or phenomena creating noise pulses and accidental coincidences, so that a bias level for acceptance of pulses from the first two counters may easily be set somewhere between the two groups of pulse heights (plateau measurement). The bias level for acceptance of pulses from the third counter is set as low as possible, just above the noise level, so that it counts a particle that just emerges from the ΔR foil. (See Ashby[21] for analysis of plateau measurement and discriminator bias adjustment.)

D. Electronics

The hv supply is a 0-2 kv photomultiplier supply furnishing 1100 v to operate the three proportional counters. The signal from each counter goes through a pre-amplifier to a linear amplifier (LA) (See Fig. 3). The individual gains of the linear amplifiers are set to account for any difference in gas multiplication that might exist in the counters. In practice very little difference in setting is observed. The pulses from the linear amplifiers, set so that the largest are just overloading, enter variable gate (VG) and delay units where the acceptance biases, delays, and pulse lengths for the coincidence circuits are adjusted. The pulses from LA 1 and 2 are made 0.5 μsec long and the pulse from LA 3 is made 1.5 μsec, overlapping 1 and 2 on each side in time. The timing is set with a pulser fed through the linear amplifiers. The jitter in time of the pulses from the first two proportional counters has been measured to be about 0.05 μsec, a very small part of the pulse widths. The jitter of 3 with respect to 1 and 2 is another story, however, being about 0.5 μsec. An overlap of 0.75 μsec is found to cover this sufficiently. The VG gate pulses are mixed in one quad of an eight-channel quadruple mixer. The coincidences and singles are monitored with scalers. A fourth VG and delay unit is fed with the input signal for VG 2. The pulse is delayed several μsec and fed into the second quad of the eight-channel mixer along with normal pulses from VG 1 and 3. The rate of accidental coincidences may be monitored in this way. All electronics is standard Radiation Laboratory design.

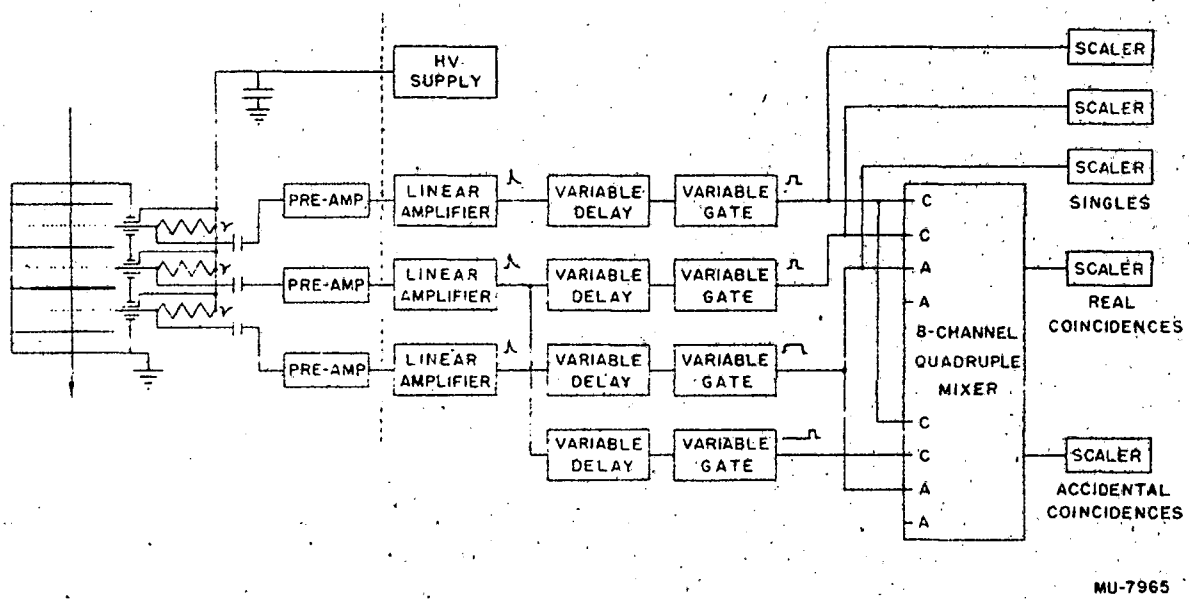

Fig. 3. Electronics block diagram.

E. Beam Integrator

The beam is collected in a Faraday cup[19]. The charge is integrated on a capacitor known in value to 0.1 percent. The voltage across the capacitor is measured by an electrometer and read on a recording voltmeter. All components are standard and of proven precision.

REDUCTION OF DATA

A. Range-Energy Relation

All data are taken in the form of a range spectrum--that is, the number of particles of range between R and R+ΔR passing through the solid-angle-defining collimator per unit charge of collected beam. Smith's range-energy plot[4] for protons in Al is used to obtain the energies of the particle groups. In addition, in order to interpolate between entries above 15 Mev, the relation

$$R = \text{antilog}\,(0.43620)\, E_{Mev}^{1.778} + 2.0\ \text{mg/cm}^2\ \text{Al}$$

was derived from entries at 15, 23, and 32 Mev and fits all intermediate entries to ± 0.2 mg/cm^2.

B. Transformation: Laboratory to Center-of-Mass System

The transformation from the laboratory frame to the center-of-mass frame of reference utilizes the nonrelativistic formulas,

$$\tan\theta = \frac{\sin\phi}{\cos\phi + r},$$

$$\cos\phi = \cos\theta\sqrt{1 - r^2\sin^2\theta} - r\sin^2\theta,$$

$$\sin(\phi - \theta) = r\sin\theta, \text{ and}$$

$$\frac{\Delta\omega}{\Delta\Omega} = \frac{\sin\phi\,\Delta\phi}{\sin\theta\,\Delta\theta} = \frac{(r\cos\theta + \sqrt{1 - r^2\sin^2\theta})^2}{\sqrt{1 - r^2\sin^2\theta}},$$

and the equivalent mass ratio r is given in general by

$$\frac{1}{r^2} = \frac{M_2 M_4}{M_1 M_3}\left[1 + \frac{M_1 + M_2}{M_2}\,\frac{Q - \epsilon}{E_o}\right]$$

where the reaction is

$$M_1 + M_2 + (KE)_o \rightarrow M_3 + M_4 + (KE)_f + \epsilon;\ (M_1 \text{ is bombarding particle})$$

and

$Q = (M_1 + M_2) - (M_3 + M_4)$

ϵ = nuclear excitation energy

E_o = lab energy of incoming proton (= KE_o)

θ = lab angle

ϕ = center-of-mass angle

$\Delta\Omega$ = solid-angle increment (lab)

$\Delta\omega$ = solid-angle increment (c.m.)

C. Expression for Energy of Scattered Particles

From the kinematics of the general collision, the lab-system energy of a particle of mass M_3 scattered at the lab angle θ from a particular reaction is

$$E_\theta = \frac{M_3 M_1}{(M_1 + M_2)^2} \frac{E_o}{r^2} \left[r \cos\theta + \sqrt{1 - r^2 \sin^2\theta} \right]^2$$

For protons elastically scattered from Be^9, to find E_o from E_p, knowing ϕ,

$$E_o = \frac{100}{81} E_p \frac{\sin^2\theta}{\sin^2\phi}$$

For deuterons leaving Be^8 in its ground state, to find E_o from E_d, knowing ϕ,

$$E_o = -0.61 \text{ Mev} + \frac{100}{72} E_d \frac{\sin^2\theta}{\sin^2\phi}$$

D. Excitation Energy

A formula giving the excitation energy of a level, if the difference in energy (ΔE) between the group corresponding to the level and the group corresponding to the ground state at the angle θ is known, is

$$\epsilon = \frac{M_1 + M_2}{M_4} \Delta E - \frac{M_1 M_3}{M_4(M_1 + M_2)} E_o \cos\theta \left(\frac{1}{r} - \frac{1}{r'}\right)\left(1 + \frac{1}{2} r r' \sin^2\theta\right),$$

where an approximation $\sqrt{1 - x} = 1 - 1/2\, x$ (for $x < 0.07$) is made in the second term. The approximation influences ϵ by less than 0.1 percent in the worst case. The value of r' (the equivalent mass ratio for the inelastic collision) includes a guess for the ϵ. The calculated value of ϵ is very insensitive to the accuracy of this guess. An average value of E_o may also be used.

E. Differential Cross Section

The differential cross section (c.m.) corresponding to a particle group at θ is given by the relations

$$\frac{d\sigma}{d\omega} = \frac{d\sigma}{d\Omega} \frac{\sin\theta \, d\theta}{\sin\phi \, d\phi},$$

$$\frac{d\sigma}{d\Omega} = \frac{1}{\Delta\Omega N_p N_T} \frac{\cos \theta/2}{t} \frac{A}{\Delta R},$$

where A = area of peak $\frac{(\text{counts mg/cm}^2 \text{ Al})}{\mu\text{coulomb}} = \frac{1}{CV} \int \left[\frac{dN}{dR} \Delta R\right] dR$,

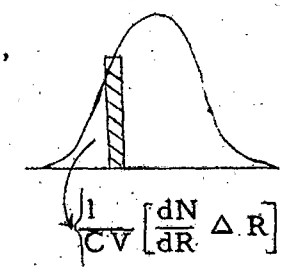

N_p is the number of protons per μcoulomb,

N_T is the number of nuclei in the target per mg,

t is the thickness of the target foil in mg/cm^2

$\Delta\Omega$ is the solid angle of the detector,

ΔR is the differential range foil thickness in mg/cm^2 Al,

C is the beam collection capacitor (μfarads),

V is the electrometer reading (volts),

so that $$\frac{d\sigma}{d\omega} = \left(\frac{e M_{Be} \times 10^9}{\Delta\Omega \, \Delta R \, t}\right) A \frac{\cos \theta/2 \sqrt{1 - r^2 \sin^2\theta}}{\left[r \cos\theta + \sqrt{1 - r^2 \sin^2\theta}\right]^2} \text{ cm}^2/\text{steradian}$$

where e is the electronic charge in coulombs, and

M_{Be} is the mass of the Be^9 atom in grams.

F. Rutherford Scattering Formula. Target Thickness

A convenient general form for the Rutherford scattering cross-section formula for protons of energy E_o (Mev) on target Z^A is

$$\frac{d\sigma}{d\omega} = 1.28 \times 10^{-27} \frac{Z^2}{E_o^2} (1 + \frac{1}{A})^2 \frac{1}{\sin^4 \phi/2} \text{ cm}^2/\text{steradian}.$$

Integrating this to find the number scattered beyond a certain angle ϕ_o and setting this equal to 1 percent of the incident particles, we can solve

for the thickness of a target that will scatter less than 1 percent of the incident protons outside the angle ϕ_o:

$$t = \frac{1033\ \text{mg/cm}^2}{\langle R \rangle} E_o^2 \frac{A-2}{Z^2} \frac{\cos \theta/2}{\left[\frac{1}{\sin^2 \phi_o/2} - 1\right]} \left(\text{neglecting } \frac{1}{A^2} \text{ w.r.t. } \frac{1}{A}\right),$$

where $\langle R \rangle$ is an average ratio to Rutherford scattering (experimental) for Z.

G. Discussion of Errors

All figures are for the 24-in. scattering chamber.

The calculation of the value of the absolute differential cross section corresponding to a particle group at θ depends upon the following measured quantities,

$$\frac{d\sigma}{d\omega} \sim \frac{A}{\Delta\Omega\Delta R} \frac{\cos \theta/2}{t} \frac{d\Omega}{d\omega}(\theta),$$

so that

$$\frac{\delta\left(\frac{d\sigma}{d\omega}\right)}{\frac{d\sigma}{d\omega}} = \left[\left(\frac{\delta A}{A}\right)^2 + \left(\frac{\delta \Delta\Omega}{\Delta\Omega}\right)^2 + \left(\frac{\delta \Delta R}{\Delta R}\right)^2 + \left(\frac{\delta t}{t}\right)^2 + \left(\frac{\delta \cos \theta/2}{\cos \theta/2}\right)^2 + \left(\frac{\delta\left(\frac{d\Omega}{d\omega}\right)}{\frac{d\Omega}{d\omega}}\right)^2\right]^{1/2}$$

Now $$A = \frac{1}{CV} \int \left[\frac{dN}{dR} \Delta R\right] dR = \frac{1}{CV} \sum_i N_i \quad (dR = 1\ \text{mg/cm}^2),$$

$$\frac{\delta A}{A} = \left[\left(\frac{\delta C}{C}\right)^2 + \left(\frac{\delta V}{V}\right)^2 + \left(\frac{\sqrt{\Sigma N_i}}{\Sigma N_i - BG_i}\right)^2\right]^{1/2},$$

$$\frac{\delta C}{C} = 0.1\%,$$

$$\frac{\delta V}{V} = 0.5\%.$$

$\frac{\sqrt{\Sigma N_i}}{\Sigma (N_i - BG_i)}$ varies from 2 percent (elastic peaks) up, and is less than 5 percent in most other cases. (BG_i = background of ith point)

so $$\frac{\delta A}{A} \simeq \frac{\sqrt{\Sigma N_i}}{\Sigma (N_i - BG_i)} \text{ (statistical fluctuation)},$$

$$\frac{\delta\Delta\Omega}{\Delta\Omega} = \left[\left(\frac{2\delta d}{d}\right)^2 + \left(\frac{\delta \ell}{\ell}\right)^2\right]^{1/2} = 2.3\%,$$

$d = 0.1875 \pm .002$ in. (ID of collimator hole),

$\ell = 6.56 \pm .05$ in. (distance-- target to collimator).

After Ashby[21],

$\Delta R = 6.22 \pm .01$ mg/cm^2	aluminum foil
$0.62 \pm .06$	second counter
$0.03 \pm .02$	third counter
$6.87 \pm .064$ mg/cm^2,	

$$\frac{\delta\Delta R}{\Delta R} = 0.9\%$$

$t = 11.18 \pm .01$ mg/cm^2,

$$\frac{\delta t}{t} = 0.1\%,$$

$$\frac{\delta(\cos\theta/2)}{\cos\theta/2} = -\tan\theta/2\ \delta(\theta/2), \qquad (\theta/2) \leq 45^\circ$$

$\delta(\theta/2) \leq 3^\circ$, (nonreproducibility of target angle setting)

$$\frac{\delta(\cos\theta/2)}{\cos\theta/2} = 5\% \text{ at } \theta = 90^\circ,$$

$$\frac{\delta(d\Omega/d\omega)}{d\Omega/d\omega} = 0.1\% \text{ for } \delta\theta = 0.1^\circ \text{ (table setting).}$$

If the cross section for a reaction is changing rapidly with angle, another uncertainty becomes important which depends upon the accuracy of setting the angle of the detector. In the worst case (elastic cross section at 20° lab), the rate of change is 8 percent per degree, so that an 0.8 percent uncertainty might enter for $\delta\theta = 0.1^\circ$.

Finally, the total relative uncertainty in the value of the absolute differential cross section becomes

$$\frac{\delta\left(\frac{d\sigma}{d\omega}\right)}{\frac{d\sigma}{d\omega}} = \left[\left(\frac{\delta A}{A}\right)^2 + (2.3\%)^2 + (0.9\%)^2 + (0.1\%)^2 + (5\%)^2 + (0.8\%)^2\right]^{1/2}$$

$= 6.0\%$ for $\frac{\delta A}{A} = 2\%$ (minimum)

$= 7.5\%$ for $\frac{\delta A}{A} = 5\%$ (average).

The value for the relative error above does not contain any contribution to $\delta A/A$ by uncertainties in the points on the range spectrum due to background fluctuation or beam-energy shift. These two troubles arise from changes in accelerating conditions in the accelerator or from drift in the analyzing magnet current. Background (in the coincidence counting rate) is probably due to neutron flux through the detector, which makes (n, p) or (n, α) reactions in the separating foils so that the charged particle penetrates only the first two counters. Large shifts in background (10%) and beam energy (0.15 Mev) last only a few minutes and are easily detectable on well-defined peaks, but may cause unpredictable errors several times statistics in unfamiliar or complex portions of the range spectrum. The estimated errors in the cross sections for the higher levels (5.0 Mev and up) are based upon the possible existence of one or two spurious points in each case. No analytical expression has been derived to give this uncertainty in cross section. The experimenter, after examining many peaks on the range spectra and comparing similar portions, measures the possible outside uncertainty by eye. The probable errors in the points on the angular distributions for the higher levels are arrived at in this fashion.

Variations in the excitation energy of a level from different range spectra may be accounted for by fluctuations of the beam energy between the elastic peak and the peak corresponding to the energy level. The center of a peak may be found to within a few percent of the width of the peak in all cases in which the peak is resolved from others. The width of a peak in energy is generally less than 5 percent of the energy of the group of particles it represents, so that the energy represented by the center of the peak may be found to less than 0.1 percent or 0.03 Mev (2 mg/cm^2 Al) at 30 Mev. The error in the excitation energy of a level is the rms error from the scatter in the tabulated values. All energies of particle groups are based upon Smith's range-energy plot[4] and are limited in determination of absolute value by the uncertainties in the plot.

RESULTS AND CONCLUSIONS

A Range Spectra

Complete range spectra from the elastic peak down to about 40 or 50 mg/cm^2 Al, where α-particles make a large contribution, were obtained at 15°, 30°, 45°, 52-1/2°, 60°, 75°, 90°, and 135° (lab). (See Fig. 4.) The 15° elastic peak was incomplete but the beam energy may be determined from the deuterons from the Be^8 ground state. On the 90° spectrum the peaks are (from right to left) the elastic peak, the 2.45-Mev level, the 6.76-Mev level, the deuterons from the Be^8 ground state (the small sharp peak), and the broad 3-Mev Be^8 level with the 11.3-Mev Be^9 level superimposed at the same range, suggestions of two small peaks not outside statistics (possible 14.5- and 17.5-Mev levels), and the 19.9-Mev Be^9 level just as the three-body inelastic protons and alphas start to rise markedly.

The portion of the range spectrum between excitations (Be^9) of 2.5 and 9 Mev was examined with particular care at 45° (Fig. 5), 120°, 135°, and 150° (Fig. 6) to verify structure around the 6.8-Mev level.

Elastic peaks and first-level Be^9 were taken alone at some intermediate angles to fill in angular distributions (Figs. 8 and 9).

The spectrum of He ions (see p.45, Fig. 18) was obtained at 30° by decreasing the gain of all linear amplifiers by a factor of 4. At this gain, stopping protons and deuterons give pulses too small to count, and pulses due to α's are reduced in size to that of protons with normal gain.

The Be^9 impurity elastic peaks were examined twice at 60° (Figs. 4 and 7), and a small portion of the range spectrum from ground to 8-Mev excitation of protons scattered from an oxygen gas target was obtained at the same angle.

B. Energy Levels

A tabulation of the energies and corresponding excitation energies of the different particle groups at the various angles appears in Table I (the entries below the elastic protons and "elastic" deuterons are the beam energies for these peaks).

The value for the excitation energy of the 5.0-Mev level was taken from the small portion of the 45° spectrum obtained with good statistics

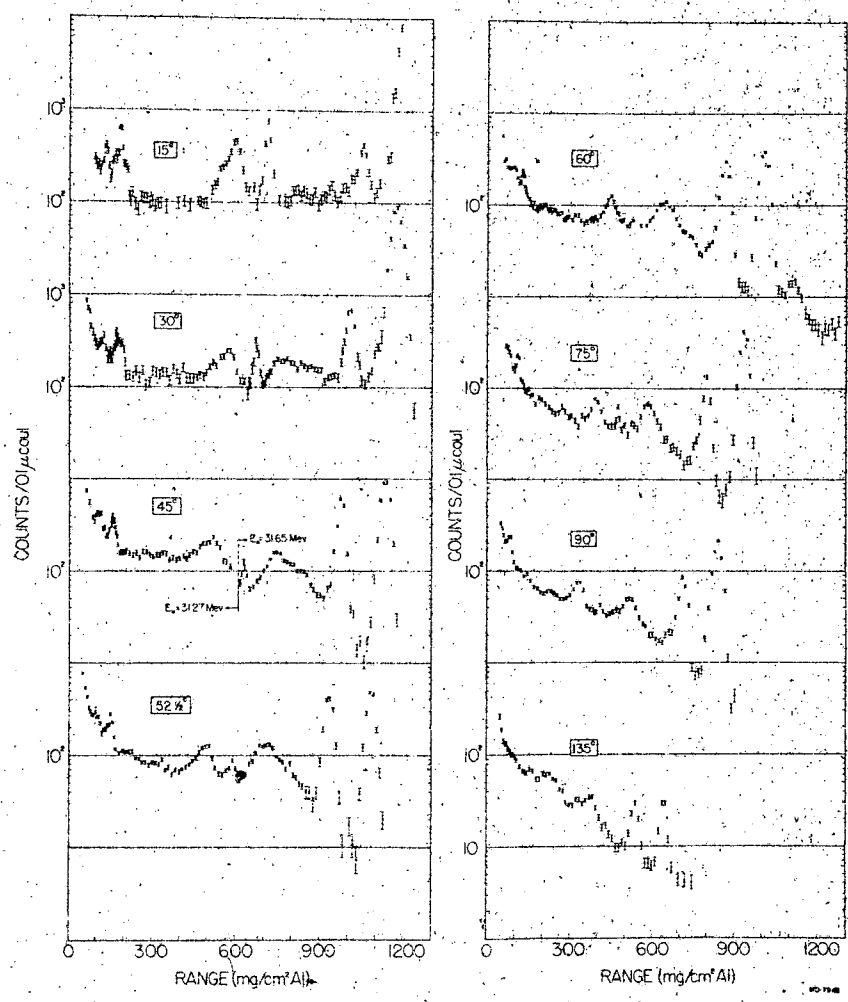

Fig. 4. Composite of range spectra of charged particles from bombardment of Be^9 by ~31.3-Mev protons, observed with the differential-range proportional counter telescope. (Ordinate is in arbitrary units.)

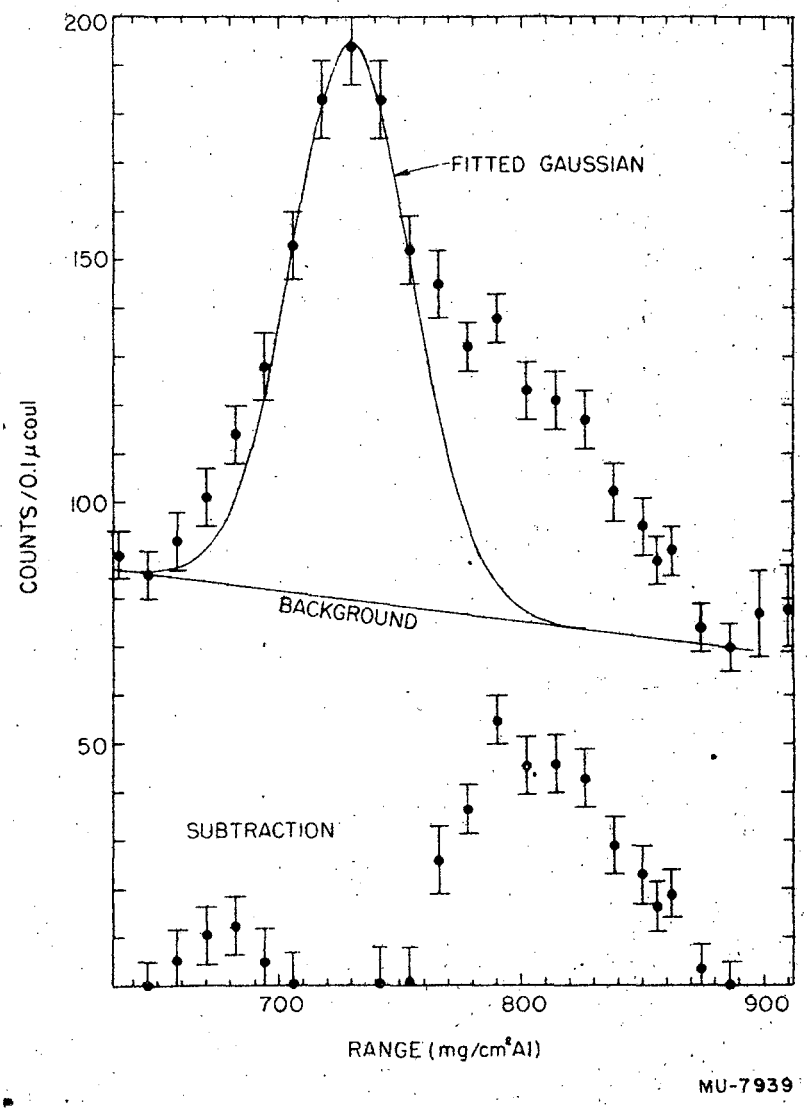

Fig. 5. Portion of 45° range spectrum in vicinity of 6.76-Mev level (solid curve), showing evidence for existence of a 5.0-Mev Be^9 excited state (subtraction curve).

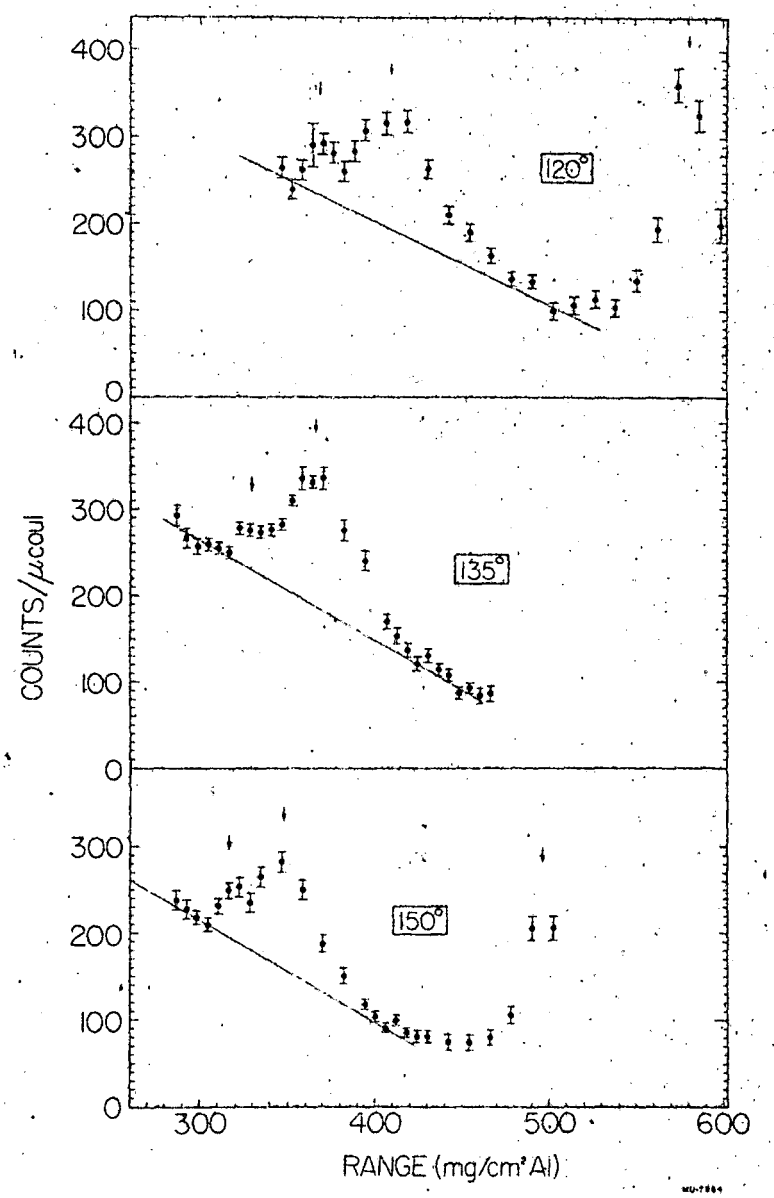

Fig. 6. Similar portions of 120°, 135°, and 150° range spectra in vicinity of 6.76-Mev level, showing evidence for existence of a 7.94-Mev Be^9 excited state (peak at left). Peak at far right is 2.45-Mev level.

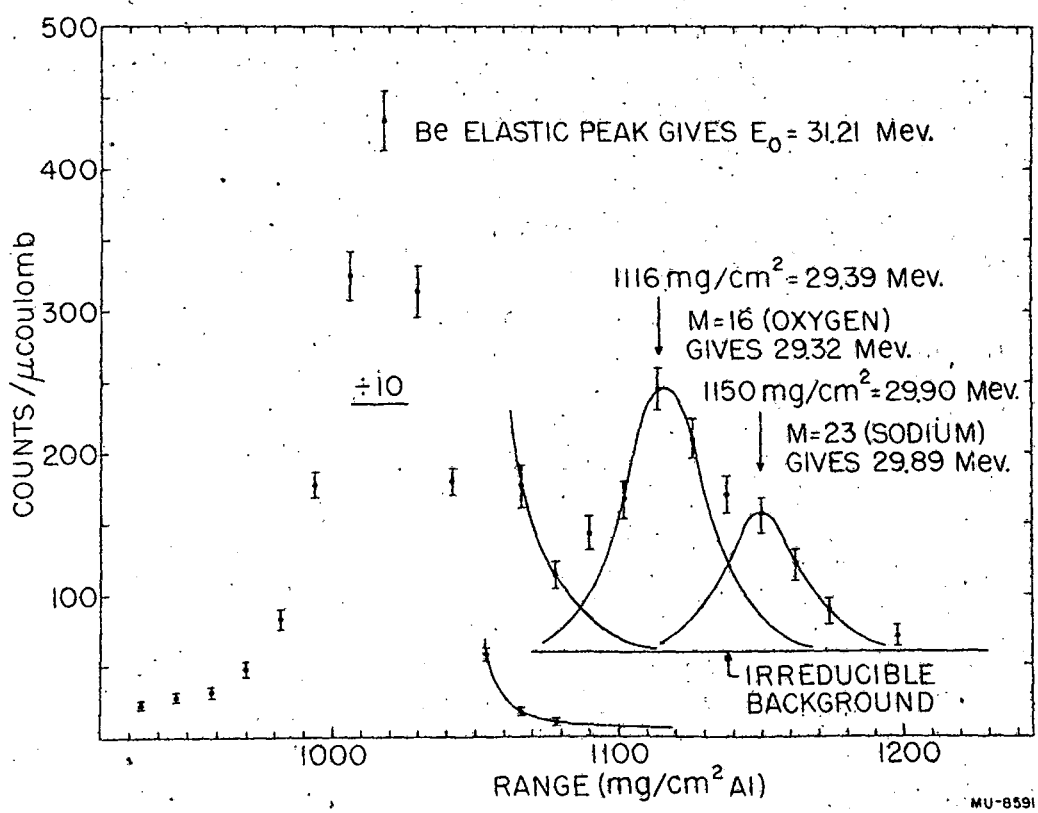

Fig. 7. Beryllium elastic peak and spectrum of longer-range protons elastically scattered from impurities at 60° (lab).

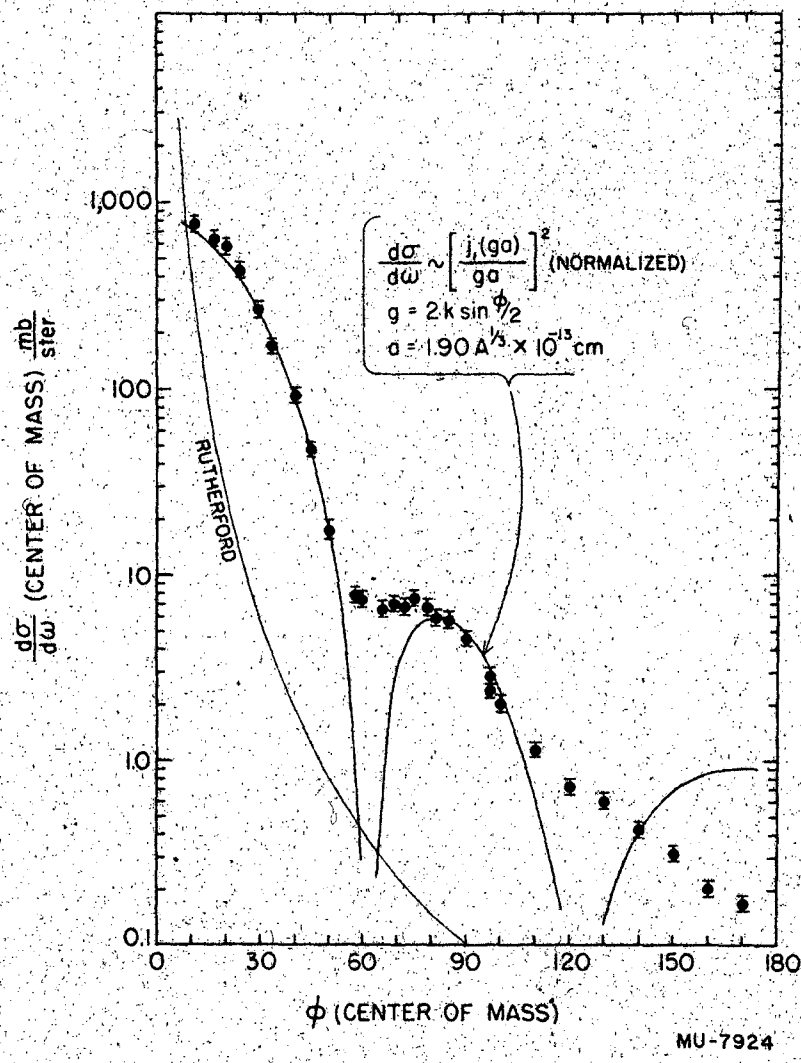

Fig. 8. Angular distribution of the differential cross section for elastic scattering of protons from Be^9 at 31.3 Mev (lab) and the Born approximation prediction for $r_o = 1.90$. (Curve not corrected for finite angular resolution of 1.6°.)

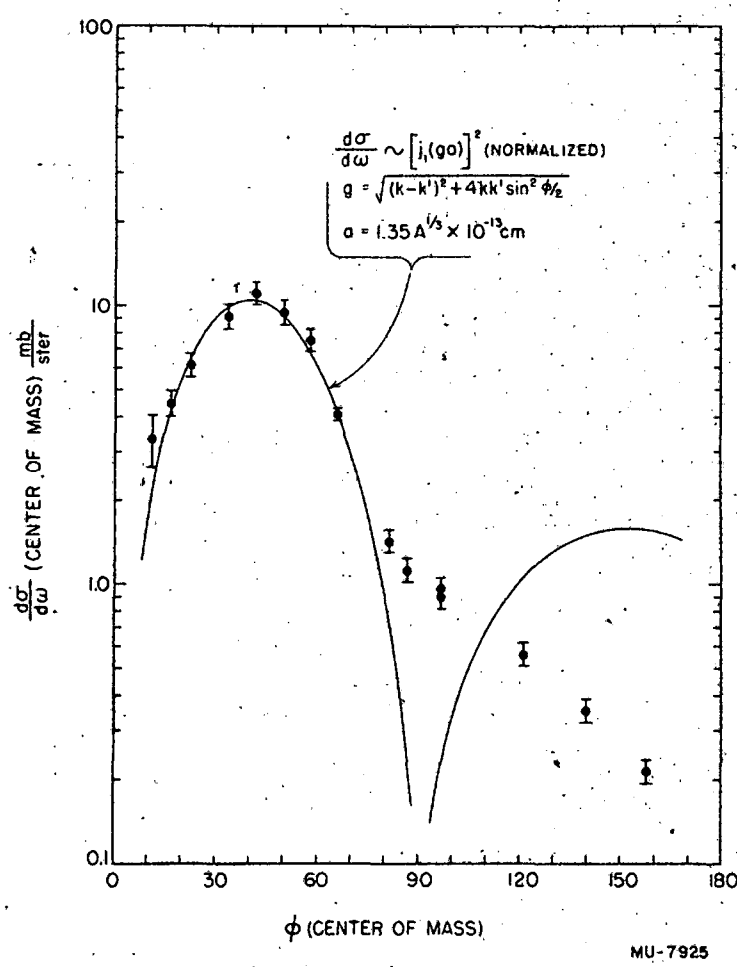

Fig. 9. Angular distribution of the differential cross section for the reaction p(31.3 Mev) + $Be^9 \rightarrow p' + Be^{9*}$ (2.45 Mev) and the Austern-Butler-McManus curve for $\ell = 1$ and $r_o = 1.35$. (Curve not corrected for finite angular resolution of 1.6°).

TABLE I

Energies of Peaks and Excitations

Angle	P_o E_o	P_1	P_2'	P_2	P_2''	D_o E_o	D_1	P_3	P_6	P_7
15°	(30.82)	28.30	26.43	24.61		30.60	27.62	19.52	10.35	8.51
	31.06	2.52	4.38	6.20		31.06	3.20	11.20	19.94	21.64
30°	30.22	27.68		23.94		29.66	27.12	18.99	10.08	8.20
	31.14	2.57		6.33		31.13	2.77	11.25	19.88	21.64
45°	29.65	27.21	24.30	23.36		28.60				
	31.65	2.51	5.49	6.45		31.62				
"	29.29	26.93		22.96		28.20	25.62	18.07	9.56	7.66
	31.27	2.42		6.49		31.17	2.88	11.45	19.88	21.71
"	(29.42)		24.49	23.14		28.42				
	31.41		5.06	6.44		31.41				
52½°	28.89	26.56	23.74			27.60	25.02		9.45	7.49
	31.52	2.42	5.34			31.54	2.92		19.84	21.76
60°	27.70	25.42		21.47		(26.18)	23.72	16.73	8.55	
	30.96	2.40		6.53		31.02	2.84	11.47	19.84	
75°	26.56	24.30		20.35	19.19	24.44			7.78	(6.25)
	31.33	2.44		6.69	7.94	31.38			20.10	(21.72)
90°	25.20	23.04		19.15	18.12	22.44	19.96			
	31.50	2.40		6.72	7.87	31.45	3.10			
"	25.02	22.80		19.01	17.88	22.48	19.88		(6.63)	
	31.28	2.47		6.68	7.93	31.49	3.25		(20.43)	
120°	(22.45)	20.33		16.69	15.72					
	31.38	(2.45)		6.80	7.96					
135°	21.49	19.46		15.89	14.82					
	31.46	2.45		6.78	8.09					
"	(21.31)			15.67	14.74					
	31.19			6.83	7.98					
150°	(20.70)			15.20	14.40					
	31.39			6.80	7.84					
Wtd. Average		2.46	5.0	6.76	7.94		2.99	11.34	19.91	21.69
Error (rms)		.05	0.3	0.06	0.08		0.17	0.12	0.09	0.05
Number		(10)	(1)	(7)	(7)		(7)	(4)	(6)	(5)

Energies in parentheses uncertain or not measured directly.

(see Fig. 5). The subtraction curve is not as clean in shape as desired and has a large half width. A statistically poor portion of range spectrum at 15° yields a much lower excitation (~4.3 Mev), different by more than an estimated error from the value at 45°. The possibility of the existence of two levels here is not remote, but due to the low cross section and unresolvable nature of the levels an attempt to establish more than one was not made.

The reader will note that at small angles (< 60°) the excitations corresponding to the 6.76-Mev level in the table are lower in value and increase with angle to 75° and remain constant thereafter. This behavior could be explained by the existence of a "6.2-Mev" level mixing with the 6.76-Mev level only at low angles, having the peak in its angular distribution at a more forward angle than that for the 6.76-Mev level (see Section D). The half width of the peak obtained from the 45° portion (Fig. 5) is wider than the instrumental width. Besides being explained by a mixture of two levels this can be accounted for by a large neutron width of the level (if it decays by neutron emission), since it is 5.2 Mev above the threshold for neutron emission. Doubt is cast on the latter explanation, however, because the particle width does not seem to increase noticeably with excitation to higher levels above the neutron threshold.

The 7.94-Mev level is observed at intermediate and backward angles and the portions of range spectra at 120°, 135°, and 150° serve to verify its existence (see Fig. 6). It is narrower than the 6.76-Mev level, and no ambiguity exists between values at different angles.

The existence of the 11.3-Mev level would have been rather hard to establish with the range method alone at this energy, as the deuterons from the 3-Mev Be^8 level splash across its position in range at nearly all angles. Rough subtraction curves are drawn to determine its position at low angles where partial resolution is possible.

There is an uncertainty about the nature of the peaks at very low energy (very high excitation). The existence of a narrow level in Be^8 at 17 Mev which decays by gamma emission is well known.[15] An attempt to match the variation in energy with angle of the very sharp peak on the range spectra with this level was made. As can be seen in Table II, the

TABLE II

High Levels as Deuterons and Tritons

Angle	D_o E_o	P_6	P_7	D_4	D_5	$D_4 = T$	$D_5 = T$	Calculated Triton Energy
[illegible]°	30.60	13.86	11.38	14.54	12.88	17.22	15.27	18.23
	31.06	17.49	19.95	16.81	18.46			
30°	29.66	13.50	10.96	14.54	13.77	17.22	16.27	17.20
	31.13	17.19	19.77	16.15	16.91			
45°	28.20	12.78	10.24	12.88	11.38	15.27	13.50	15.67
	31.17	16.88	19.54	16.77	18.35			
52 1/2°	27.60	12.64	10.02	12.00		14.25		15.00
	31.54	16.67	19.48	17.36				
60°	(26.18)	11.42		9.60	7.72	11.34	9.18	13.86
	31.02	16.77		18.77	20.82			
75°	24.44	10.42	8.34					
	31.38	16.66	19.09					
90°	22.48	(8.80)						
	31.49	(17.10)						

Entries below the energies of the deuteron groups are the excitation energies of levels of Be^8.

agreement between the excitations obtained from the very well defined energies of this peak is rather poor. On the other hand the assumption that this is a level in Be^9 leads to more consistent values for the excitation energy (19.9 Mev). The same method of identification is used for the 21.7-Mev Be^9 level although the determination is not quite so distinct because of a very much larger width.

There can be seen, just to the left of the 3.0-Mev Be^8 level in the 75°, 90°, and 135° range spectra, two small peaks definitely not outside statistics but very suggestive because of the consistency of the excitation energies obtained from their centers. Further work should be done to prove or disprove the existence of levels here (14.5- and 17.5-Mev Be^9).

Oxygen is known[15] to have levels at 6 and 7 Mev. If this element occurred in any great concentration in the Be foil, the peaks corresponding to these levels would appear mixed with the Be^9 levels of similar excitation. The range spectrum at 60° was therefore investigated above the elastic peak (see Figs. 4 and 7) for peaks due to elastic scattering of protons from heavier nuclei, and small peaks were found that are due to M = 16 (oxygen) and M = 23 (sodium). A gaseous oxygen target was then bombarded with protons of the same energy and the range spectrum at the same angle was observed from the elastic peak to excitation of about 8 Mev.

The ratio of the cross sections of the 6- and 7-Mev levels to that of the elastic scattering was obtained, and on the basis of the area of the oxygen impurity peak an upper limit for the contribution of the oxygen levels to the Be inelastic spectrum could be estimated. A value of about one fifth of the 5.0-Mev Be^9 level cross section at this angle was obtained for both levels together. The accuracy of statements about the 5.0-Mev level has been taken to include this uncertainty.

C. Angular Distribution of Elastic Scattering

The differential cross section for elastic scattering has been measured with good certainty at 28 angles at small intervals between 10° and 170°, and an experimental angular distribution is plotted (Fig. 8). By varying the value for the nuclear radius one could obtain a good fit of

$\left[\frac{j_1 (2ka \sin \phi/2)}{2ka \sin \phi/2}\right]^2$ to the data at forward angles with a between 1.85 and 2.00 $A^{1/3} \times 10^{-13}$ cm, with a best fit for $a = 1.90\ A^{1/3} \times 10^{-13}$ cm. The large value for the nuclear radius is considered to be due to assuming the Born approximation, and is probably not a measure of the actual nuclear size.

D. Angular Distributions of Inelastic Scattering

The differential cross section for inelastic scattering of protons at many different angles from Be^9, resulting in its excitation to all its known levels, has been measured. Angular distributions for each level are obtained, and although uncertainties as high as 50 percent or even an order of magnitude are estimated for some of the groups that are unresolved or of low cross section, sufficiently well-defined shapes result so that comparison may be made with the simple theory of peripheral scattering proposed by Austern, Butler, and McManus.[23] They give $\frac{d\sigma}{d\omega} \sim \left[j_\ell (ga)\right]^2$. In this expression a is a measure of the radius of the nuclear shell in which the inelastic collision takes place, and ℓ is the change in angular momentum of the scattered proton or the change in the orbital angular momentum between the ground state and the level produced. In general, the total angular momentum of the level J' may be any integral (or half integral if the ground state total angular momentum J is half integral) number between $J-\ell-1$ and $J+\ell+1$. (The spin of the proton makes a contribution of ± 1 or 0.) The parity of the wave function for the excited state is different (ℓ odd) or the same (ℓ even) as that of the ground state. For the ground state of Be^9, $J = 3/2^-$.[15]

The cross section for the 2.45-Mev level is well defined at most angles, and a good angular distribution was obtained. Figure 9 illustrates that j_1 gives a very good fit with

$$r_o = 1.35 \text{ where } a = r_o A^{1/3} \times 10^{-13} \text{cm}.$$

A poorer fit was found for $r_o = 1.30$ or 1.41. Thus $J' = 1/2, 3/2, 5/2,$ or $7/2$, all even parity ($\ell = 1$). The prediction of the α-particle model is $5/2^-$.[15] An attempt was made to fit the data with $\ell = 2$, which could give $J = 5/2^-$, requiring a larger nuclear radius for the argument of the Bessel function (to agree with elastic scattering and some other levels

giving $r_o \sim 1.8$). The best fit to the data ($r_o = 2.00$) gave a much too sharp angular distribution and passed through only three or four points near the peak of the distribution. On this evidence, the conclusions were drawn that this level has even parity, in contradiction to the prediction of the α-particle model, and that the r_o obtained with the Born approximation may not necessarily be the same for all levels as well as elastic scattering.

In spite of poor cross-section measurements and the possibility of a mixture of levels, a fit for the 5.0-Mev angular distribution was made with j_1 and $r_o \sim 1.36$ (Fig. 10). If there are two levels here, one or both are characterized by $\ell = 1$ because the cross section drops off so rapidly after 50° (c.m.), but the value of r_o might be a little different. In any case, $J' = 1/2$, $3/2$, $5/2$, or $7/2$, with even parity.

For the 6.76-Mev level, where evidence is stronger for the existence of two levels, a single-level assumption leads to a good fit with j_1, but with an extremely small nuclear radius, $r_o = 1.17$. To fit the data well using a larger nuclear radius requires the use of two values of ℓ. The two angular distributions, chosen to fit also the behavior of the excitation energy with angle (Table I), have $r_o = 1.46$ for both. The sum curve is a very good fit for the experimental points (Fig. 11). For a single level, $J' = 1/2$, $3/2$, $5/2$, or $7/2$, with even parity. For two levels, the "6.2-Mev" level has this angular momentum and parity and the 6.76-Mev level has $J' = 1/2$, $3/2$, $5/2$, $7/2$ or $9/2$ and odd parity.

The 7.94-Mev level has a very low cross section (~0.1 mb/ster. maximum) and the estimated error is rather high. From the general location of the experimental points and the knowledge that the cross section is even smaller at forward angles, one can see that a higher ℓ is required. A fit is obtained with j_3 and $r_o = 1.36$ (Fig. 12). A lower ℓ would require a smaller r. The figure of $r_o = 1.36$ is about a minimum for $\ell = 3$; a fit could still be obtained with $r_o = 1.46$, or for $\ell > 3$, with $r_o = 1.8$ to 2.0. The weight one should put on the location of the points at backward angles is questionable. However, with $\ell = 3$, $J' = 1/2$, $3/2$, $5/2$, $7/2$, $9/2$, or $11/2$, with even parity.

The cross section for the 11.34-Mev level, while being almost impossible to determine at intermediate angles because of deuterons,

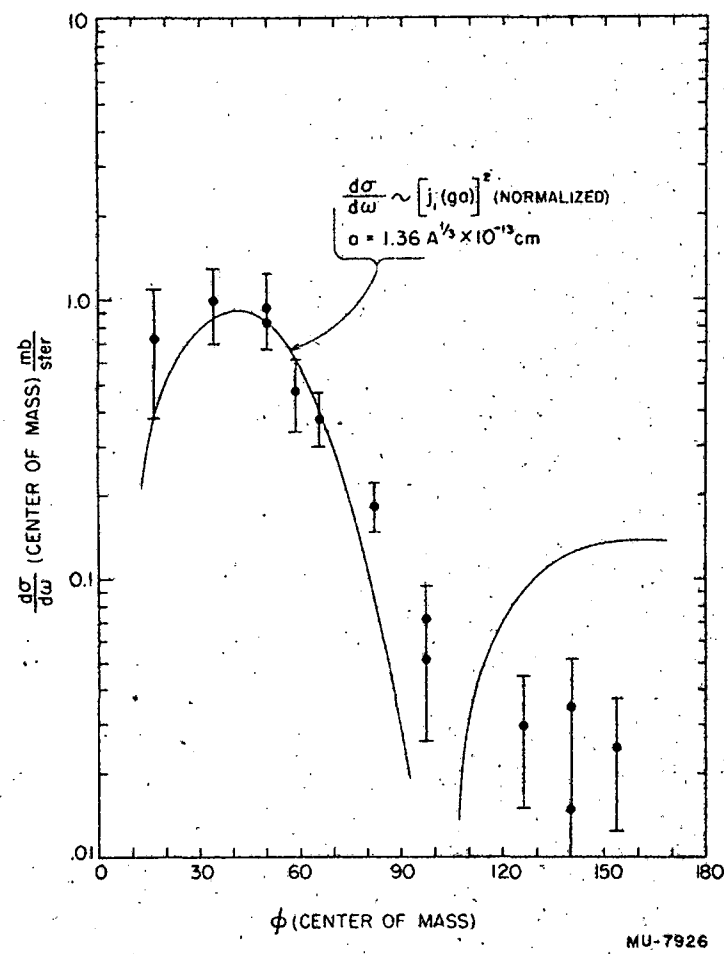

Fig. 10. Angular distribution of the differential cross section for the reaction p(31.3 Mev) + Be^9 → p' + Be^{9*} (5.0 Mev) and the Austern-Butler-McManus curve for $\ell = 1$ and $r_o = 1.36$.

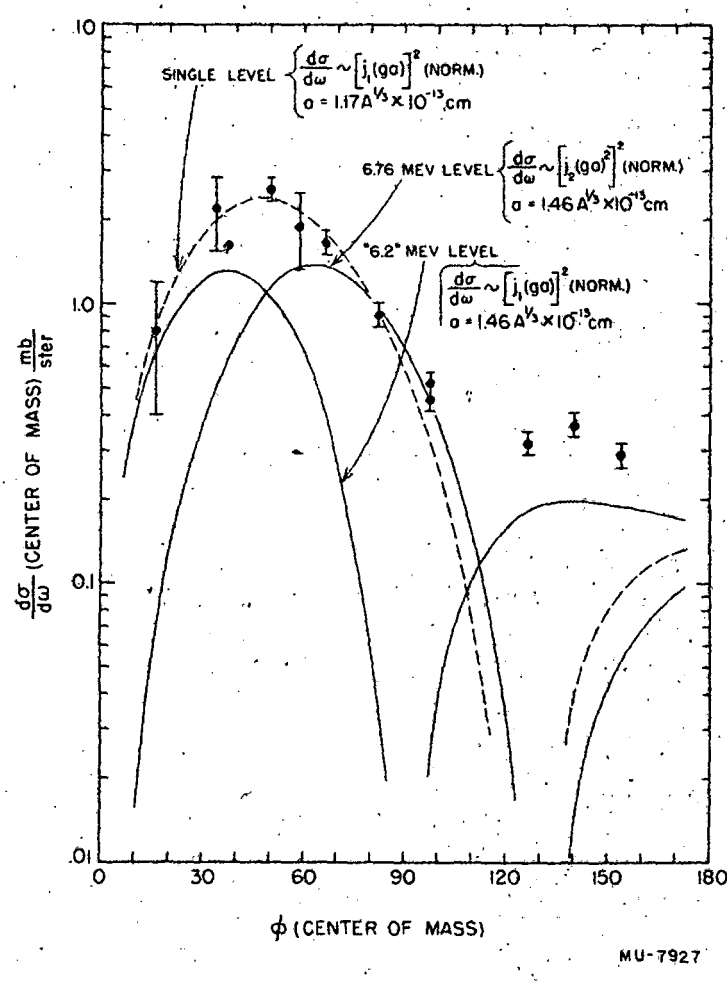

Fig. 11. Angular distribution of the differential cross section for the reaction p(31.3 Mev) + $Be^9 \rightarrow p' + Be^{9*}$ (6.76 Mev and possible "6.2 Mev" unresolved) and the Austern-Butler-McManus curves for the two cases - single level, $\ell = 1$ and $r_o = 1.17$ (dotted), and two unresolved levels with different ℓ (2 and 1) and same $r_o = 1.46$ (solid curve).

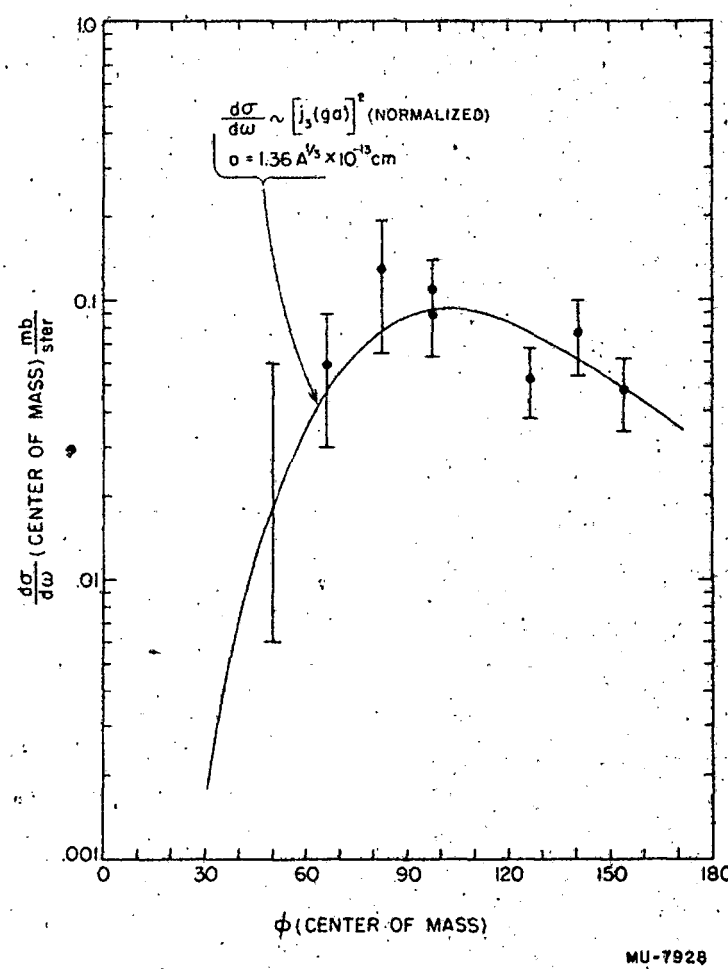

Fig. 12. Angular distribution of the differential cross section for the reaction p(31.3 Mev) + $Be^9 \rightarrow p' + Be^{9*}$ (7.94 Mev) and the Austern-Butler-McManus curve for $\ell = 3$ and $r_o = 1.36$.

is definitely increasing toward forward angles, indicating $\ell = 0$. An attempt to fit the experimental points leads to a choice for the nuclear radius which is either very large or very small, $2.00 < r_o < 1.10$ (Fig. 13). Since the 19.9-Mev level gives a larger radius, the value $r_o = 2.00$ is preferred even though further work is indicated here. If $\ell = 0$, $J' = 1/2$, $3/2$, or $5/2$, with odd parity.

The angular distribution for the 19.9-Mev level is unquestionably $\ell = 0$ (peaked forward) and $r_o = 1.81$. The fit is quite good and the experimental points are well determined (Fig. 14). This level and the 2.45-Mev level show that the peripheral scattering theory may yield quite a variation in r_o for the different levels. For the 19.9-Mev level, $J' = 1/2$, $3/2$, or $5/2$, with odd parity.

Large errors in the 21.7-Mev level cross section make a match difficult. Since the distribution is undoubtedly peaked forward, $\ell = 0$ is first indicated, but since the theoretical distributions travel forward with increasing excitation, $\ell = 0$ gives a much too steep distribution with a decreased r_o. A fit is made with $\ell = 1$ and $r_o = 1.70$ (Fig. 15). The resulting J' is $1/2$, $3/2$, $5/2$, or $7/2$, with even parity.

The fit given by this theory at forward angles is unquestionable for the levels whose cross section is well determined, and it is felt that definite information about levels may be obtained with this method, even though the question about the wandering nuclear radius is unanswered (cf. section C, Angular Distribution of Elastic Scattering).

A summary of the results for the various levels is as follows:

ϵ (in Mev)	ℓ (in $\hbar$)	r_o
2.46 ± 0.05	1	1.35 ± .02
5.0 ± 0.3	1	1 36 ± .05
6.76 ± 0.06 (and "6.2")	2 (and 1)	1.46 ± .03
7.94 ± 0.08	3	1.36 ± .15
11.34 ± 0.12	0	1.10 ± .1 or 2.00 ± .1
19.91 ± 0.09	0	1.81 ± .03
21.69 ± 0.05	1	1.70 ± .1

E. Angular Distributions of Deuteron Groups

The angular dependence of the differential cross section for observation of the reactions Be^9 (p, d) Be^8 and Be^9 (p, d) Be^{8*} (3.0 Mev) is plotted in Figs. 16 and 17. Attempts were made to fit the ground-state group

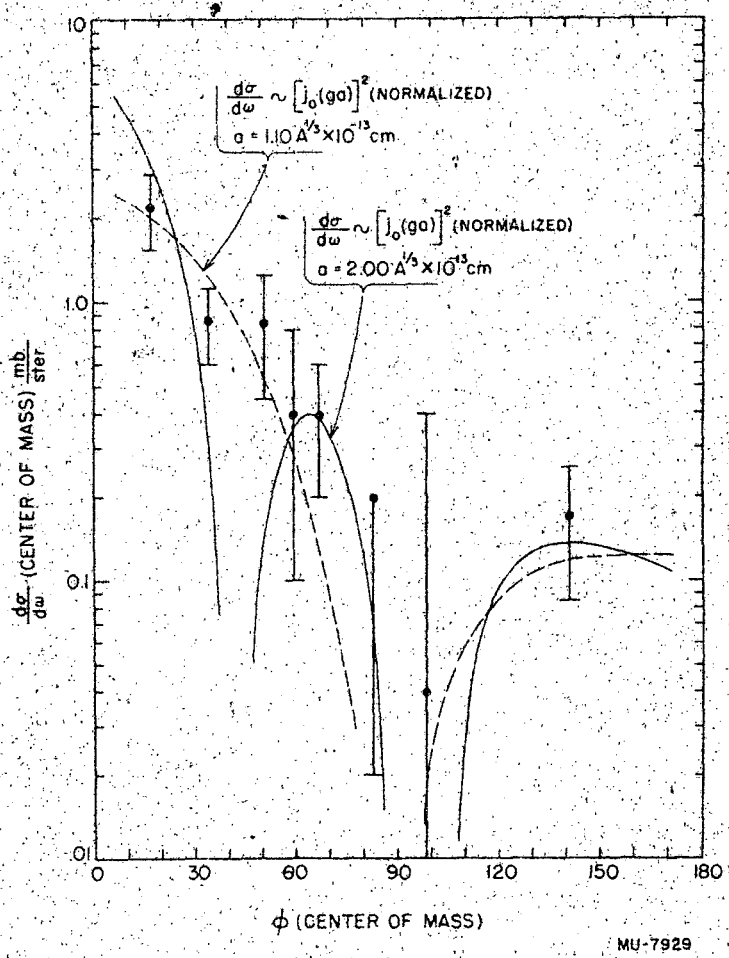

Fig. 13. Angular distribution of the differential cross section for the reaction p(31.3 Mev) + $Be^9 \rightarrow p' + Be^{9*}$ (11.3 Mev) and the Austern-Butler-McManus curves for $\ell = 0$ (both) and $r_o = 1.10$ (dotted) and 2.00 (solid).

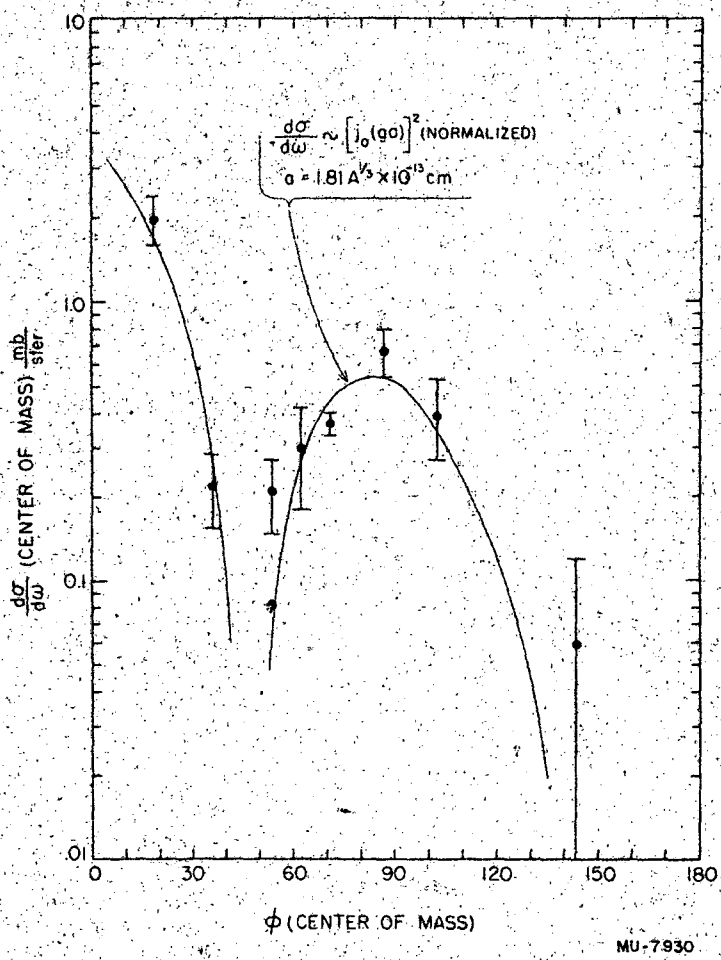

Fig. 14. Angular distribution of the differential cross section for the reaction p(31.3 Mev) + $Be^9 \rightarrow p' + Be^{9*}$ (19.91 Mev) and the Austern-Butler-McManus curve for $\ell = 0$ and $r_o = 1.81$.

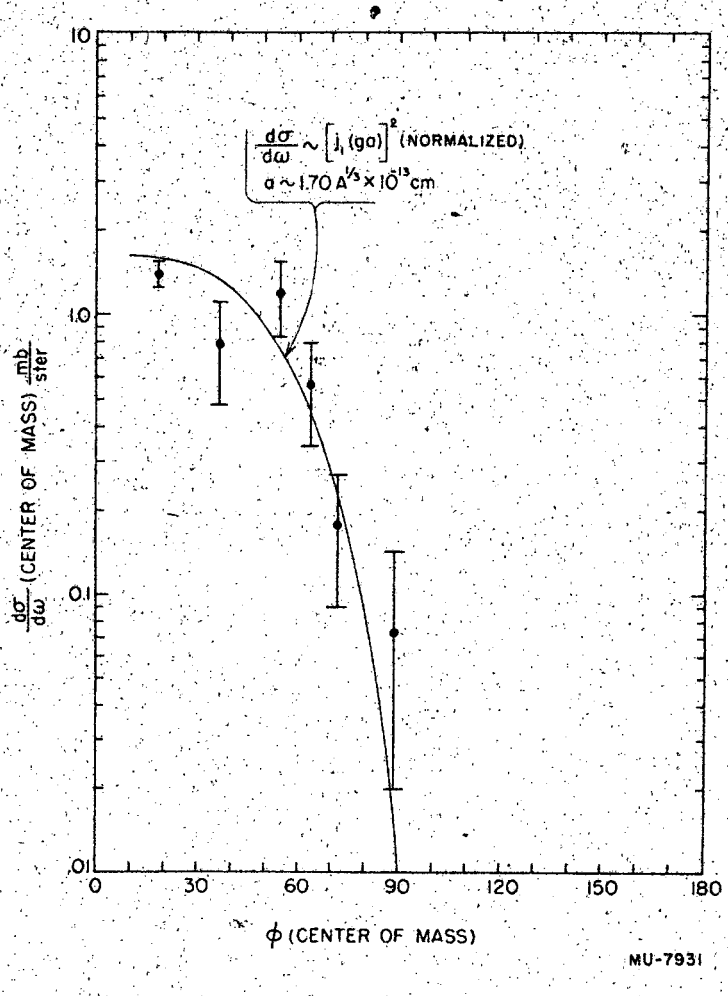

Fig. 15. Angular distribution of the differential cross section for the reaction p(31.3 Mev) + $Be^9 \rightarrow p' + Be^{9*}$ (21.7 Mev) and the Austern-Butler-McManus curve for $\ell = 1$ and $r_o = 1.70$.

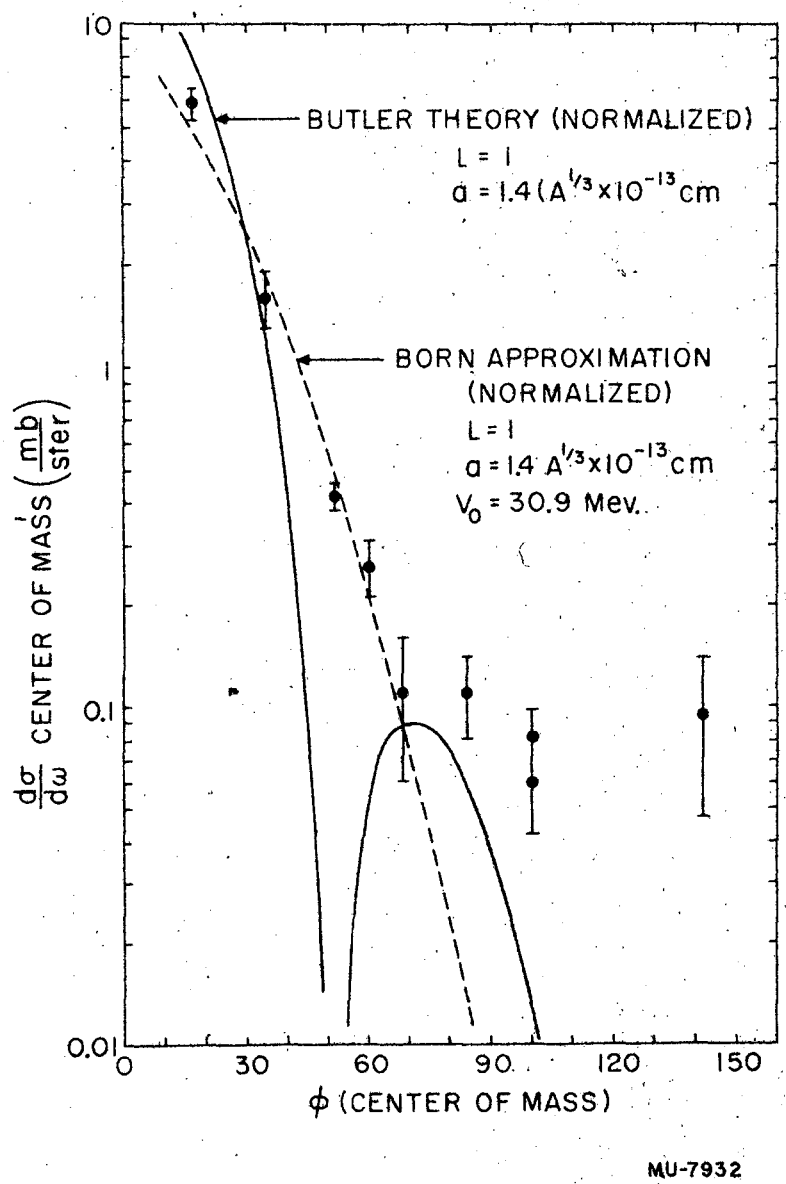

Fig. 16. Angular distribution of the differential cross section for the reaction p(31.3 Mev) + Be^9 → d + Be^8, the Butler theory prediction (solid curve), and the Born approximation (Daitch and French) curve (dotted).

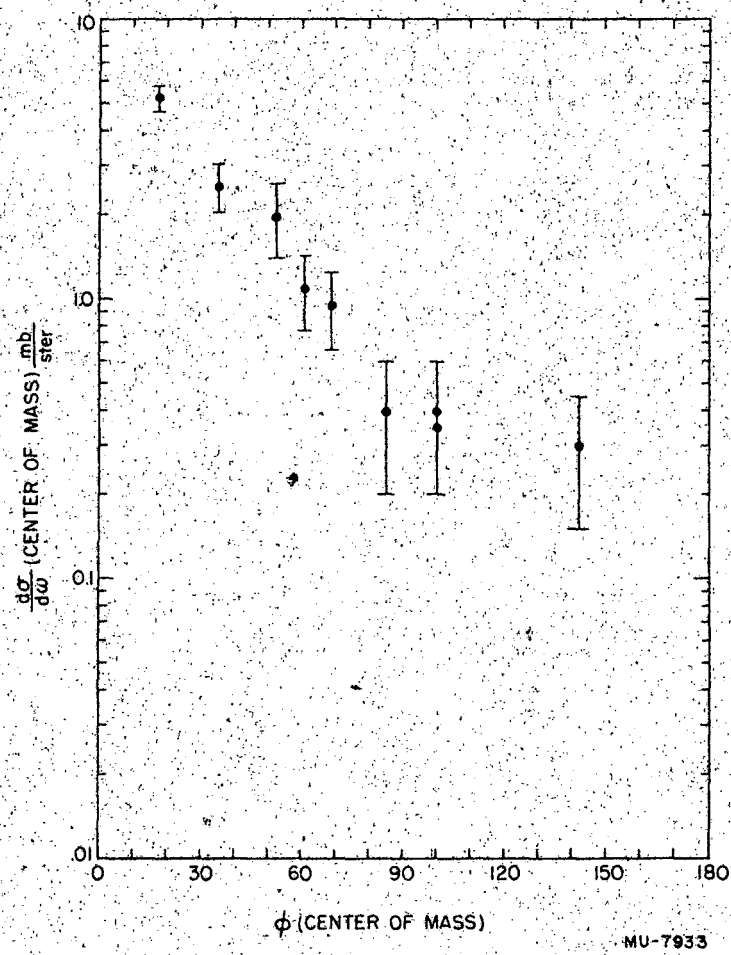

Fig. 17. Angular distribution for the differential cross section for the reaction p(31.3 Mev) + $Be^9 \rightarrow d' + Be^{8*}$ (3.0-Mev level).

angular distribution with normal Butler theory predictions for $\ell = 0$, 1, and 2 in each case. The best fit (and not a good one) is obtained with $r = 1.4\ (A^{1/3} + 1) \times 10^{-13}$ cm and $\ell = 1$, in good agreement with the known change in J from $3/2^-$ (Be^9) to 0^+ (Be^8). If, however, we consider the possibility that the proton may pick up a neutron anywhere throughout the nuclear volume (proposal of Daitch and French[26]) the integral in the Born approximation is taken over the whole nucleus instead of just a shell. This extension of the limits brings a factor into the angular distribution (see Appendix) with a singularity which may wipe out one of the minima and give a distribution such as we find in Fig. 16. The parameters for this curve are $r = 1.4\ A^{1/3} \times 10^{-13}$, $\ell = 1$ as before, and the nuclear energy-well depth for the neutron $V_o = 30.9$ Mev.

The 3.0-Mev level angular distribution can be fitted by no Butler theory expression for $\ell = 0$, 1, 2, or 3 with any acceptable value for the nuclear radius. The cross section decreases with increasing angle much more slowly than any prediction. In this case Butler theory may break down because the width of the 3-Mev level is so large.

F. Other Particles

A negative result was obtained in a search of the low-energy peaks from the data at different angles for a peak exhibiting the energy-vs.-angle dependence of tritons from Be^9 (p, t) Be^7 ground state. In Table II are listed the energies of possible groups as tritons and the energy predicted for tritons at that angle and beam energy from the kinematics of the reaction. There is no obvious correlation. No attempt was made to detect tritons by dE/dx measurements. The existence of monoenergetic tritons is certainly probable, but the present data are too incomplete to verify it.

He^3 and alphas, although hard to distinguish from each other, are easily separable from protons, since their dE/dx is about four times as large. The range spectrum at 30° of particles of charge two (or greater) is plotted in Figure 18. No structure is evident that would identify the ground state of Li^6 or Li^7. The energy resolution of the detector is probably too poor to see any distinct group.

The range of the Li^6 recoil at 15° is about the same as the minimum

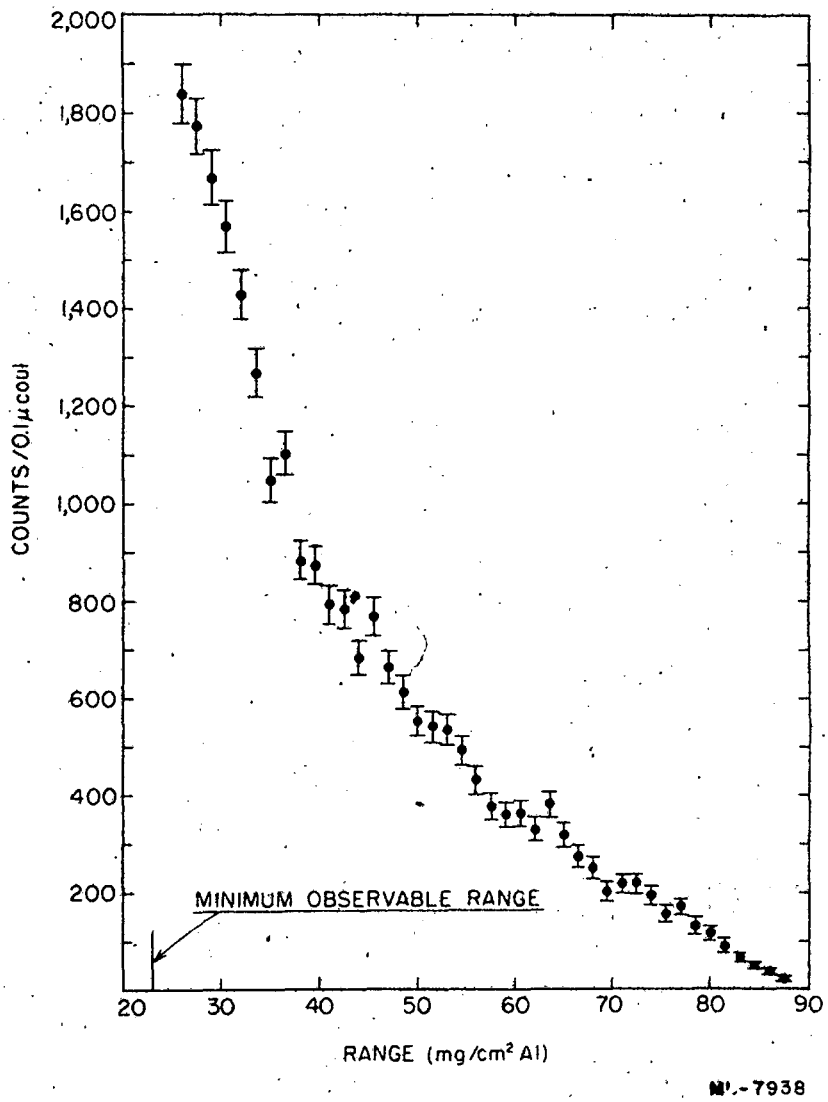

Fig. 18. Range spectrum of He (and heavier) ions from p(31.3 Mev) + Be^9 at 30° (lab).

observable range, but no attempt has yet been made to detect this ion although it should have a dE/dx about twice that of an α and be easily separable. Since the counter telescope can be easily modified to decrease its minimum range and improve the resolution at these ranges, a future investigation of the He and heavier recoil-ion spectrum would be quite feasible at this beam energy.

ACKNOWLEDGMENTS

The author is indebted to

Professor L. W. Alvarez for his interest and encouragement,

Dr. Jacob Benveniste for his guidance, inspiration, and active participation in all phases of this experiment,

Dr. E. A. Martinelli for his participation at the inception and guidance throughout the experiment,

Dr. Warren Heckrotte for many inspiring discussions on angular distributions,

William Gantz and Thomas Stand of Mr. H. Farnsworth's Electronics Group for their expert maintenance of the electronic equipment,

Manuel M. Alcalde for the fabrication of the counter box,

Earl Hostetter, who skillfully constructed the grids for the counters,

William G. Richards for his suggestions and help in constructing the remainder of the equipment made for this experiment,

And, finally, all members of the linear accelerator crew, without whose patience and cooperation the successful completion of this experiment would not have been possible.

This work was done under the auspices of the U. S. Atomic Energy Commission.

APPENDIX

General Butler Theory Angular Distribution[11,22] (nonrelativistic)

$$\left(\frac{d\sigma}{d\omega}\right)_\ell \sim f(K)\left[A_\ell j_\ell(Zr) + B_\ell\left(\frac{Zr}{2\ell+1}\right)\left\{\ell j_{\ell-1}(Zr) - (\ell+1) j_{\ell+1}(Zr)\right\}\right]^2,$$

where

$$f(K) \sim \left\{\frac{1}{K^2+a^2} - \frac{1}{K^2+(a+b)^2}\right\}^2 \quad \text{(Fourier transform of deuteron wave function)},$$

$$K = \sqrt{(\tfrac{1}{2}k_d - k_p)^2 + 2k_d k_p \sin^2 \phi/2},$$

$$a = 2.32 \times 10^{12}\ \text{cm}^{-1}$$

$$b \simeq 6a$$

$$Z = \sqrt{(k_d - k_p)^2 + 4k_d k_p \sin^2 \phi/2}$$

r = radius of nucleus plus radius of deuteron

$$\simeq 1.4\,(A^{1/3}+1) \times 10^{-13}\ \text{cm}$$

$$A_\ell = \sum_{n=0}^{\ell} \frac{(\ell+n)!\,(k_s r + n + 1)}{n!\,(\ell-n)!\,(2k_s r)^n}$$

$$B_\ell = \sum_{n=0}^{\ell} \frac{(\ell+n)!}{n!\,(\ell-n)!\,(2k_s r)^n}$$

$$ik_s = k_n$$

$$k_{d,p,n} = \sqrt{\frac{2M_{d,p,n}E_{d,p,n}}{\hbar}}$$

$E_n = E_d - Q - E_p$ (center-of-mass energies)

$Q = 2.22$ Mev

Correction factor given by Daitch and French[26]

$$\hat{F} = \frac{1}{\left(\frac{\hbar^2 K^2}{2M_d} - V_o\right)}$$

V_o = energy-well depth of nucleus for neutrons.

REFERENCES

1. T. R. Wilkins and G. Kuerti, Phys. Rev. 57, 1081, 2 (1940).
2. C. F. Powell, A. N. May, J. Chadwick, T. G. Pickavance, Nature 145, 893, 901 (1940).
3. R. H. Dicke, and J. Marshall, Phys. Rev. 63, 86 (1943).
4. J. H. Smith, Phys. Rev. 71, 32 (1947).
5. K. E. Davis and E. M. Hafner, Phys. Rev. 73, 1473 (1948).
6. C. Longmire, Phys. Rev. 74, 1773 (1948).
7. S. Fernbach, R. Serber, and T. B. Taylor, Phys. Rev. 75, 1352 (1949).
8. E. H. Rhoderick, Proc. Roy. Soc. (London) A201, 348 (1950).
9. C. Levinthal, E. A. Martinelli, and A. Silverman, Phys. Rev. 78, 199 (1950).
10. V. F. Weisskopf, Helv. Phys. Acta 23, 187 (1950).
11. S. T. Butler, Proc. Roy. Soc. (London) A208, 559 (1951).
12. J. A. Harvey, Phys. Rev. 82, 298 (A) (1951).
13. J. M. Blatt and V. F. Weisskopf, "Theoretical Nuclear Physics", Wiley, (1952) p. 535.
14. R. E. LeLevier and D. S. Saxon, Phys. Rev. 87, 40 (1952).
15. F. Ajzenberg and T. Lauritsen, Revs. Modern Phys. 24, 321 (1952).
16. Roy Britten, Phys. Rev. 88, 283 (1952).
17. J. C. Arthur, A. J. Allen, R. S. Bender, H. J. Hausman, and C. J. McDole, Phys. Rev. 88, 1291 (1952).
18. K. E. Davis, Phys. Rev. 88, 1433 (1952).
19. J. Benveniste, "Inelastic Events Induced by 32-Mev Protons on Helium", University of California Radiation Laboratory Report No. UCRL-1689, March 31, 1952.
20. J. Benveniste and B. Cork, Phys. Rev. 89, 422 (1953).
21. V. J. Ashby, "Differential Cross Section for the Elastic Scattering of 32-Mev Protons by Deuterons", January 28, 1953, UCRL-2091.
22. E. Gerjuoy, Phys. Rev. 91, 645 (1953).
23. N. Austern, S. T. Butler, and H. McManus, Phys. Rev. 92, 350 (1953).
24. R. M. Eisberg and G. Igo, Phys. Rev. 93, 1039 (1954).
25. Gerhard E. Fischer, "The Scattering of 10-Mev Protons on Carbon and Magnesium", University of California Radiation Laboratory Report No. UCRL-2546, April 1954.
26. P. B. Daitch and J. B. French, Phys. Rev. 87, 900 (1952).